

TOPOLOGY DESIGN AND FREEFORM FABRICATION OF DEPLOYABLE STRUCTURES WITH LATTICE SKINS

Uma Maheshwaraa, Carolyn Conner Seepersad, and David Bourell
Mechanical Engineering Department
The University of Texas at Austin, Austin, TX 78712

Abstract

Solid freeform fabrication is particularly suitable for fabricating customized parts, but it has not been used for fabricating deployable structures that can be stored in a compact configuration and deployed quickly and easily in the field. In previous work, lattice structures have been established as a feasible means of deploying parts. Before fabricating the parts with a selective laser sintering (SLS) machine and Duraform® Flex material, lattice sub-skins are added strategically beneath the surface of the part. The lattice structure provides elastic energy for folding and deploying the structure or constrains expansion upon application of internal air pressure. In this paper, a procedure is presented for optimizing the lattice skin topology for improved overall performance of the structure, measured in terms of deviation from desired surface profile. A ground structure-based topology optimization procedure is utilized, with a penalization scheme that encourages convergence to sets of thick lattice elements that are manufacturable and extremely thin lattice elements that are removed from the final structure. A deployable wing is designed for a miniature unmanned aerial vehicle. A physical prototype of the optimal configuration is fabricated with SLS and compared with the virtual prototype.

1. Introduction

Deployable structures can be transformed from a compact configuration to a predetermined, expanded form for full functionality [1,2]. Deployment mechanisms include pneumatic arches, membranes, pantographs, and tensegrity structures, as found in applications ranging from common umbrellas to temporary shelters to expandable satellite booms for solar arrays or antennas [1,2]. Collectively, these deployment mechanisms restrict the geometry of a deployed structure to symmetric, polygonal, or spherical shapes and make it difficult to rapidly customize the geometry and functionality of the device.

To overcome these limitations, lattice skins have been introduced as a deployment mechanism, along with an accompanying solid freeform fabrication approach for realizing them. The design and freeform fabrication process is illustrated in Figure 1. Beginning with a part of arbitrary surface profile and hollow interior, lattice sub-skins are added beneath the surface of the structure, as illustrated in Steps 1 and 2. As illustrated in Figure 2, two types of lattice skins can be applied. Open lattice skins are truss-like structures that provide direct reinforcement of the surface of a part. Closed lattice structures connect the surface of a part to a concentric, inner skin. When air pressure is applied between the concentric skins, the closed lattice structures constrain expansion to maintain the desired surface profile of the part. In Step 3, the lattice structure is optimized with a topology optimization procedure described in detail in Section 2. If the part is larger than the build chamber, it is decomposed in Step 4 and fabricated as a collection of parts that are subsequently joined together. In Step 5, the part is fabricated using selective laser sintering (SLS) technology and a flexible, elastomer material called Duraform® FLEX.

Processed parts are infiltrated with polyurethane to make the structures air-tight. The flexible structure can be folded for ease of storage and transport and then deployed in the field via a combination of elastic strain energy and pneumatics. In this process, the lattice structure serves several functions. First, during the folding step, it stores strain energy that can be returned upon unfolding to help deploy the structure into its original configuration. Second, in its deployed form, the lattice structure supports the surface of the flexible part to prevent collapse and distortion of the desired surfaces. Finally, if elastic energy is insufficient for deploying a large structure under its own weight, air pressure is applied inside the structure, and the lattice skin constrains the expansion of the structure to prevent balloon-like inflation and preserve desired surface profiles. If desired, thermoset polymers or other coatings can be applied to the deployed part to rigidize it.

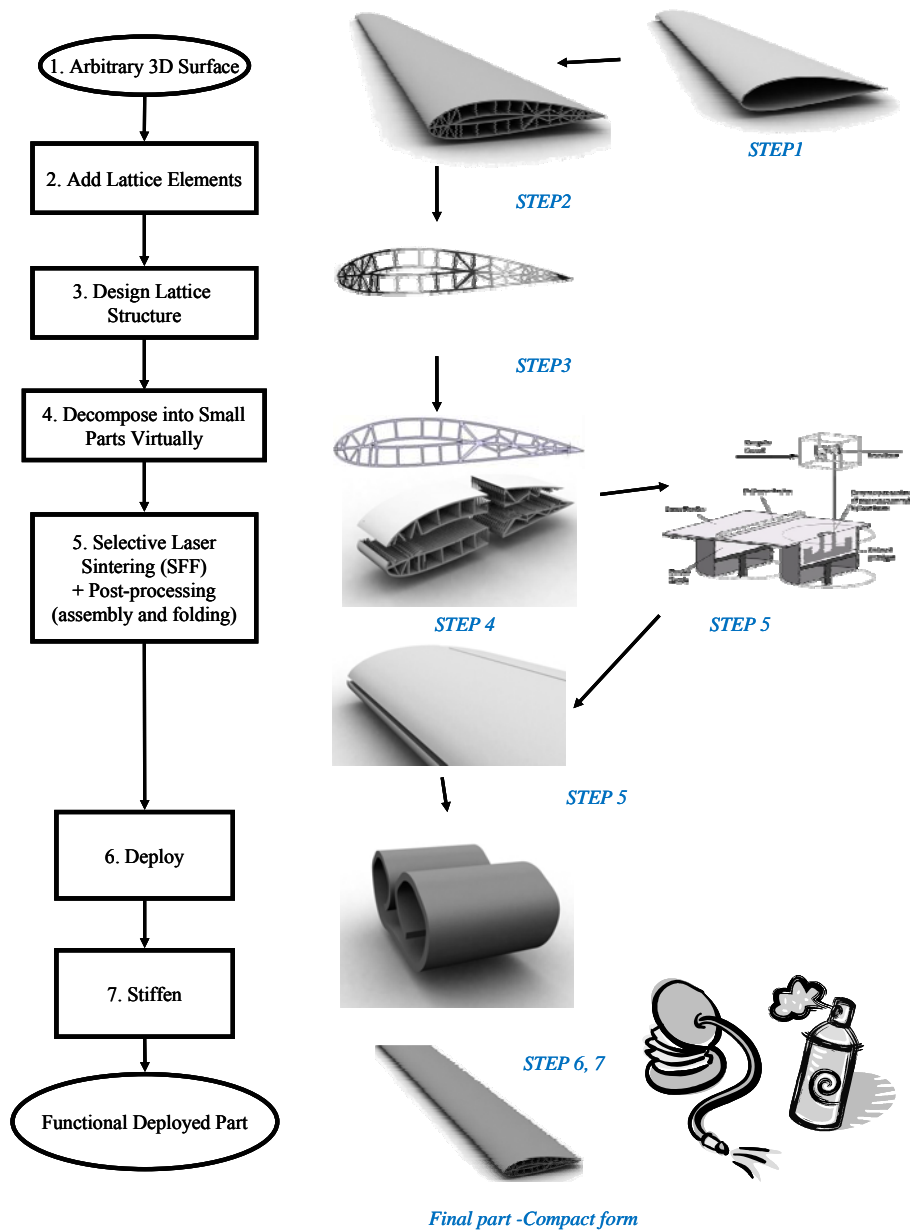


Figure 1. Design methodology for freeform deployable parts with lattice skins.

Lattice structure deployment mechanisms offer a number of advantages, relative to conventional deployment mechanisms. They provide shape control of relatively arbitrary, freeform geometries; occupy very little space in the build chamber; and do not require small-scale pivots or joints that can be difficult to fabricate and energy-intensive to deploy. They offer a combination of low relative density and high effective stiffness (a common characteristic of cellular or honeycomb materials [3]), providing high levels of rigidity for controlling deployment of a part without significantly impacting its relative density for collapsed storage and transport. The lattice skin can be used for multifunctional purposes, such as convective cooling when filled with air or blast protection when filled with earth, foam, or other materials. Finally, lattice skins are conducive to portable deployment, requiring only a portable air pump, rather than energy-intensive erection equipment or motors.

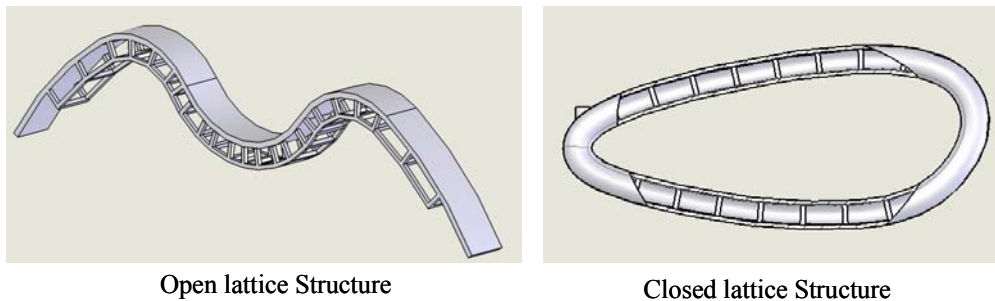


Figure 2. Open and closed lattice structures.

In previous work, feasibility studies of lattice skin deployment have been conducted, and promising results have been reported [4,5]. In this work, the focus is on topology design optimization of inflatable *closed* lattice skins for improved surface precision of deployed structures. A ground structure-based topology optimization approach is presented as a means of formalizing Steps 2 and 3 of the methodology in Figure 1. The approach is applied to the design of inflatable closed lattice structures for a UAV application.

2. Topology Optimization of Lattice Structures for Deployment

One of the most critical steps in the methodology for lattice skin deployment (Figure 1) is the design of the lattice structure (Step 3). Previous investigations have shown that the dimensions and arrangement of the lattice structure have a significant impact on the overall surface profile of the deployed part [4]. In fact, by strategically adjusting the thicknesses and configuration of the closed lattice structure for a representative airfoil part, maximum deflection on the surface of the part was reduced by more than 70% [4]. Since the dimensions and configuration of the lattice structure have such a significant impact on the surface profile of the deployed part, a formal topology design procedure has been devised for systematically designing the lattice structure.

2.1 Topology Design Optimization Procedure

As illustrated in Figure 3, a topology optimization approach has been formalized for minimizing the deflection of the part surface from its intended deployed profile. This goal is achieved by creating a lattice skin and refining its topology and dimensions. The procedure begins with a CAD file of the part. For a closed lattice configuration, a concentric skin is added beneath the

surface of the part, as illustrated in the bottom left of Figure 3. The two skins are connected with a dense grid of lattice elements. From this CAD model, an ANSYS model is created, with beam elements representing the lattice elements and 2D plane elements representing the concentric skins (for 2D cross sections, as analyzed in this application). The density of the material is used to simulate the body weight of the structure, and internal pressure is applied to simulate pneumatic inflation in the space between the concentric skins, as illustrated in Figure 4. Additional loading profiles and displacement constraints are applied, as appropriate for specific applications. Large deformation analysis capabilities are activated in ANSYS [6] because preliminary work has shown that it is necessary for accurately modeling the structural behavior of Duraform® FLEX in lattice skin applications [4]. The ANSYS model of the lattice structure is created using an APDL file. APDL is the ANSYS Parametric Design Language, a scripting language that allows the user to automate tasks and build a model in terms of variables [6]. In the APDL file, a separate variable governs the in-plane thickness of each lattice element. The APDL file is interfaced with iSIGHT design exploration software [7], which couples the analysis with an optimization algorithm. iSIGHT executes an optimization algorithm to iteratively adjust the dimensions of the lattice elements, as a means of minimizing the deflection of the outer surface of the part from its intended, deployed profile. Specifically, for each iteration of its optimization algorithm, iSIGHT adjusts the in-plane thickness of each element by updating its associated variable in the APDL file, executing the APDL file in ANSYS, and then reading the ANSYS output file to assess the impact of the change on the maximum surface deflection in the part. The optimization process in iSIGHT is a two-step procedure. A genetic algorithm is used to explore the nonlinear design space, followed by a gradient-based, sequential quadratic programming algorithm for further refining the best structure identified by the genetic algorithm. The algorithm settings are documented in [5].

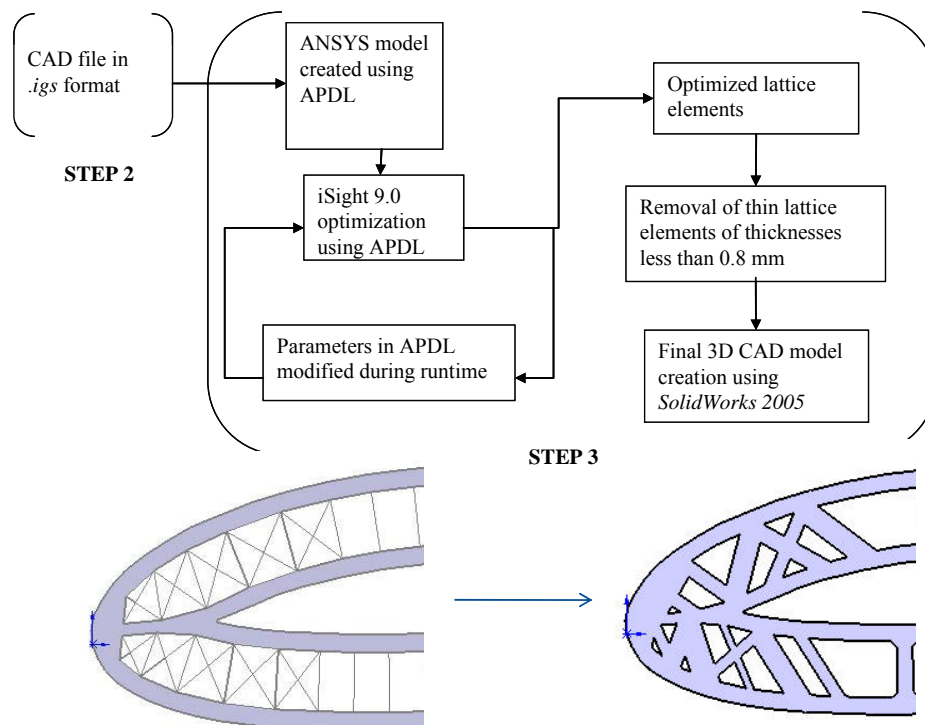


Figure 3. Topology design process [5].

Minimize
Maximum displacement, δ of any node on the outer surface

Find
Density, ρ_i , of each lattice element, i

Subject to

Bounds
 $0.0001 \leq \rho_i \leq 1.0$

Constraints
 $\nu \leq 0.5$

Calculate
Thickness (t_i) = $\rho_i \times t_{max}$
Volume fraction (ν) = $\sum \frac{\rho_i^{1/p} t_{max} \times l_i}{TotalArea}$

Constants
 l_i – length of each lattice element, i
 p – Penalty factor, $p = 3$
 t_{max} , Maximum allowable thickness, $t_{max} = 3mm$
Total Area = $\sum l_i t_{max}$

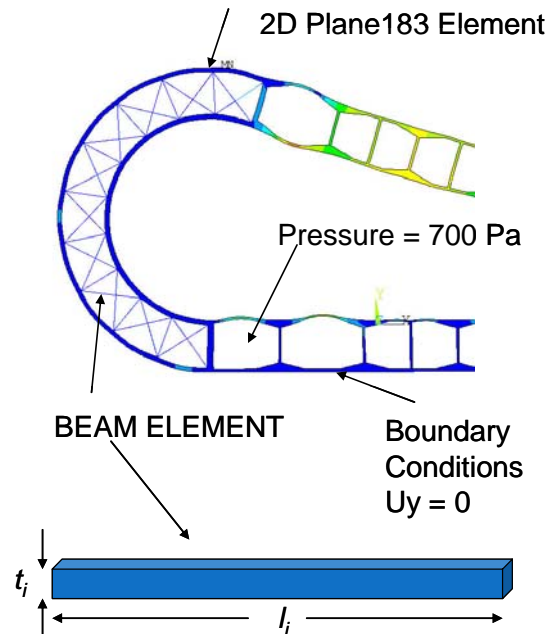


Figure 4. Topology design problem formulation and ground structure diagram.

The optimization process follows a ground structure approach [8-11], as formalized in Figure 4. The objective is to minimize the maximum displacement, δ , of any node on the outer surface of the part, thereby minimizing the deflection from the desired surface profile. The optimization algorithm adjusts the thickness of each element indirectly by varying the density, ρ_i , of each element, which is related to its in-plane thickness, t_i , according to the following relationship:

$$t_i = \rho_i t_{max}$$

where t_{max} is the maximum allowable in-plane thickness of a lattice element. During the optimization process, the lattice element densities and corresponding thicknesses are assigned large upper bounds (several mm or cm for t_{max}) and extremely small lower bounds (on the order of 1E-4 mm). A constraint is placed on volume fraction, ν , defined as the fraction of the maximum possible in-plane area occupied by lattice elements with uniformly maximum thickness. Under the restriction of the volume fraction constraint, the optimization algorithm strategically allocates material to the elements with the greatest impact on the surface deflection of the part. After the algorithm converges, elements with lower bound thicknesses are removed from the final structure because they have very little effect on the structural performance of the part. Each element removal constitutes a topology change in the lattice structure. Thick elements remain in the final lattice structure with their optimized thickness values. Elements of intermediate thickness (e.g., 0.05 mm) are not manufacturable with the SLS process, but they can have a significant collective effect on the structural characteristics of the part. Therefore, a penalty function is applied to encourage convergence to either lower or upper bounds and to discourage intermediate element thicknesses. The penalty function is implemented as part of the volume fraction constraint. The penalty factor, p , penalizes intermediate density (and thickness) elements with an artificially high contribution to the volume fraction. Accordingly, the algorithm seeks to replace intermediate density elements with thicker elements that provide greater stiffness with nearly equivalent contributions to the volume fraction.

2.1 Deployable UAV Wing Example

The research methodology is applied to design a deployable UAV wing that can be folded into a compact form and then deployed to its full size using an air pump. Several basic assumptions are made in the design of the UAV wing, as noted below and illustrated in Figure 5:

Maximum flight speed:	25 m/s
Altitude of flight:	200 m
Pressure (P_1) at 200 m:	$9.945 \times 10^4 \text{ N/m}^2$
Density of air (σ) at 200 m:	1.15 kg/m^3
Chord:	10 cm
Span:	40 cm
Required lift:	9.81 N (1 kg per wing)
Maximum wing thickness:	27 cm

The profile chosen for the aircraft cross-section is a standard wing profile, *NACA 4420*, as shown in Figure 6 [12,13]. The profile is generated using aerodynamic software developed in MATLAB [14].

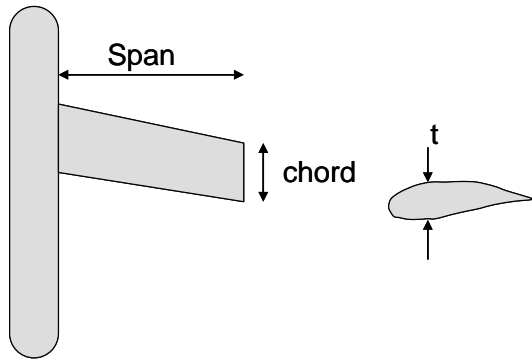


Figure 5. Wing dimensions.

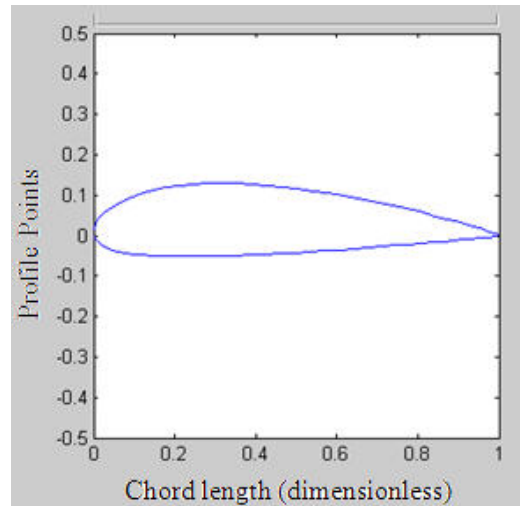


Figure 6. NACA 4420 profile, generated with MATLAB software.

UAV Wing ANSYS Modeling and Topology Optimization Setup

A dense network of lattice elements is added to the NACA 4420 model as shown in Figure 7. The inner skin and outer skin are modeled using PLANE183 area elements and the lattice elements are modeled using BEAM3 1D elements. Figure 8 shows the constraints added to the ANSYS model. The edge length for the mesh is set at 0.0005 mm and the number of finite elements in the model is 5700. Vertical displacement (y-axis) and horizontal displacement (x-axis) are constrained on the left hand side of the model. The right hand point is constrained in vertical displacement only. Air pressure is applied between the inner skin and the outer skin at 700 N/m^2 (gauge) to maintain the intended profile of the wing. The self weight of the structure is simulated by setting a gravity load in ANSYS. The aerodynamic MATLAB software calculates the coefficient of pressure (C_p) along the outer profile of the airfoil section. The coefficient of

pressure is given by Equation (2) where σ is the density of air, v_1 is the velocity of air at ambient pressure P_1 , and P is the pressure profile:

$$C_p = \frac{P - P_1}{\sigma v_1^2} \quad (2)$$

$$P_{profile} = 9.945 \times 10^4 + 0.5 \times 1.15 \times 25^2 \times C_p \quad (3)$$

Equation (2) can be rearranged to calculate the pressure profile acting on the surface of the airfoil according to Equation (3). As a worst case scenario for this analysis, the wing section is assumed to be crushed by equivalent pressure acting on the top and bottom surface.

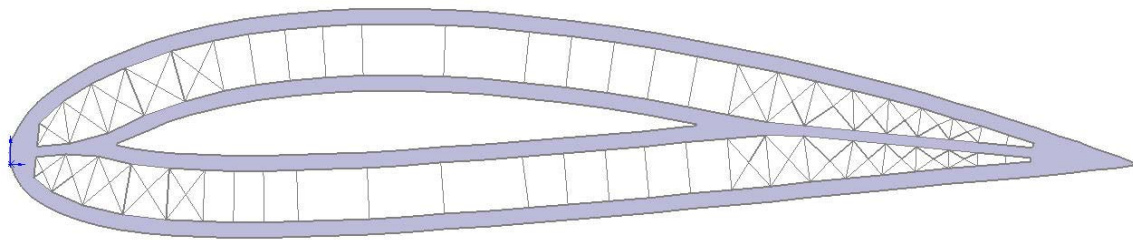


Figure 7. UAV wing profile with initial lattice structure.

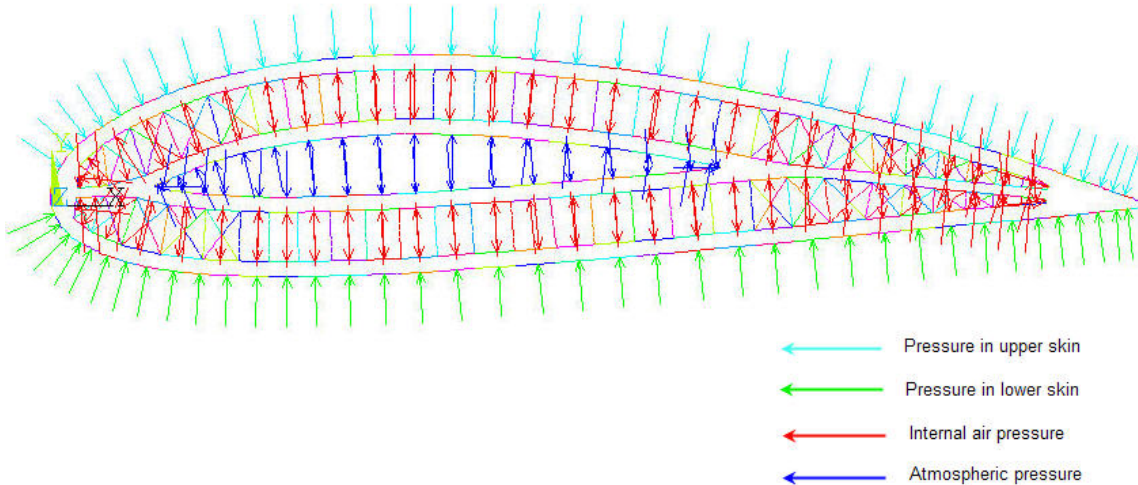


Figure 8. Pressure profile applied in ANSYS.

There are 76 lattice elements in the leading (left) and trailing (right) edges of the initial structure illustrated in Figure 9. This nonlinear problem is expensive to solve iteratively with ANSYS. To reduce computational expense, the optimization problem is split into two optimization problems. First, the UAV wing is optimized by varying the thickness of lattice elements in the left section of UAV wing. After the left section is optimized, the lattice elements in the left section are fixed with their optimal thickness values. Then, the intermediate structure is optimized by varying the lattice elements in the right section of the UAV wing. The results of the left section and right section optimizations are summarized in Table 1

Table 1. Summary of results (left and right section optimization).

	Left section optimization	Right section optimization
Number of design variables	30	46
Maximum in-plane area of lattice	491.49 mm ²	598.96 mm ²
Total iterations for convergence	1467	1146
Time taken for convergence ¹	33 hrs 24 mins	24 hrs 12 mins
Number of retained lattice elements	14	25
Final deflection	1.98 mm	1.30 mm
Final area fraction of lattice	0.24	0.32

Optimization of UAV Wing – Left Section

There are 30 elements in the initial structure of the left section of the UAV wing. Each of these elements is assigned a variable density, ρ_i . The structure is optimized according to the problem formulation in Figure 4. Figure 11 shows the retained lattice elements after the left section optimization of the UAV. The overall deflection in the UAV wing is 1.98 mm which is 65% less than the pre-optimized deflection of 6.11 mm (illustrated in Figure 10). The deflection value decreases because the optimized structure distributes material more effectively for maximum stiffness and reduced weight of the structure. The in-plane area occupied by left side elements is reduced to 118 mm² after optimization (for an area fraction of 0.24, relative to the maximum in-plane area of the elements, 491 mm², when all elements assume a maximum thickness of 3 mm).

Optimization of UAV Wing – Right Section

The overall deflection can be further minimized by optimizing the right section. During this process, the lattice elements in the left section are fixed with their optimal lattice element thickness values from the previous optimization. The number of lattice elements and associated design variables in the right section of the UAV wing is 46. Figure 13 shows the optimal configuration of the right section with 25 retained lattice elements. The deflection of the UAV cross section after right section optimization is shown in Figure 14. The deflection of the UAV wing is reduced by 33% after right section optimization. After optimization, the in-plane area occupied by right side elements is reduced to 192.97 mm² (with an area fraction of 0.32).

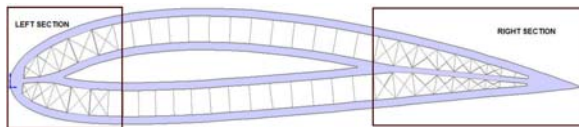


Figure 9. UAV wing with initial set of lattice elements.

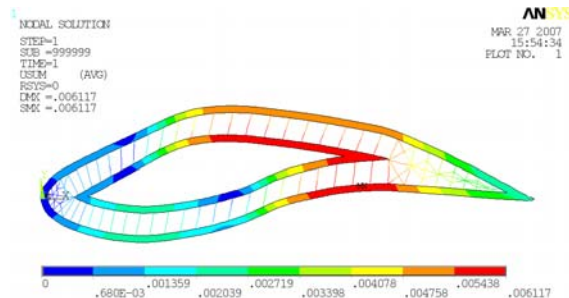


Figure 10. Deflection of UAV wing profile before optimization

¹ x86 PC running Windows XP with a 3.0 GHz dual processor and 2 GB RAM

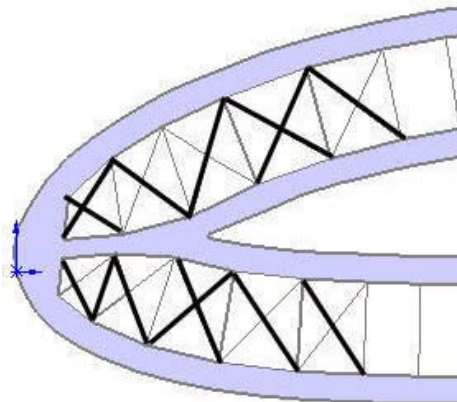


Figure 11. UAV left section optimization showing retained lattice elements in bold.

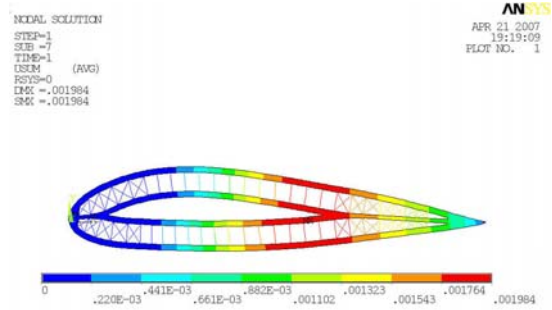


Figure 12. Deflection result of UAV WING after left section optimization.

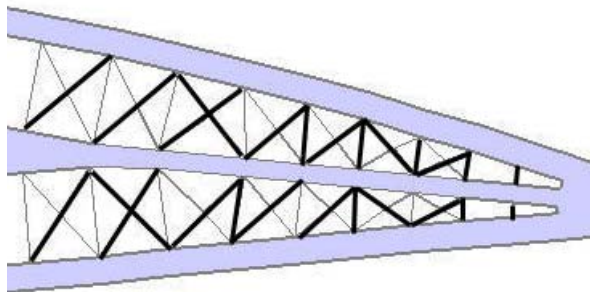


Figure 13. UAV right section optimization showing retained lattice elements in bold.

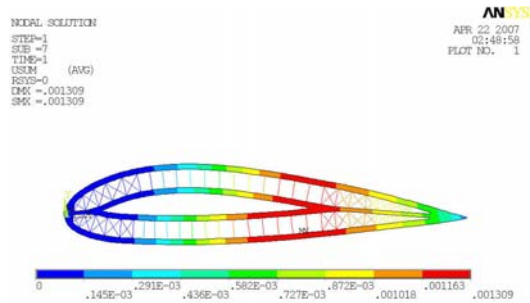


Figure 14. Deflection result of UAV WING after right section optimization.

The final lattice element configuration with 39 retained lattice elements in the left and right sections of the UAV wing is shown in Figure 15. The maximum nodal deflection of the UAV wing after optimization is improved by 78% from 6.11 mm to 1.30 mm for a structure with a maximum thickness of 27 cm and a span of 40 cm.

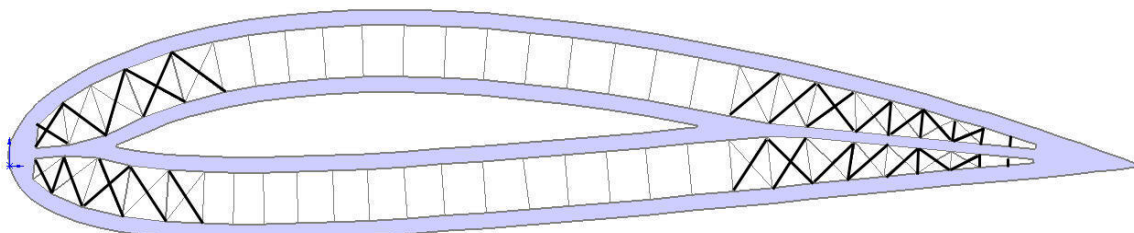


Figure 15. Final optimal lattice configuration of the UAV wing with retained elements.

2.2 Final Model and Prototype

The final model of the prototype wing is designed using SolidWorks 2005. The optimal thicknesses of lattice elements from the UAV wing optimization are used to generate the cross section of the CAD model. Figure 17 shows a section of UAV wing with the optimal lattice element thicknesses incorporated in the CAD model. The span-wise depth of the lattice

structures is 2 mm. The lattice cross-sections are repeated every 7 mm along the span of the wing to ensure that the wing can be folded. Figure 17 shows the final CAD model of the UAV wing. One end of the UAV wing is left open in the CAD model to remove unsintered powder from the internal voids. Figure 18 shows the cover to seal the open side of the UAV wing. The part is fabricated using Duraform® Flex material in an SLS machine and post-processed to remove unsintered powder. The UAV wing prototype is infiltrated using a mixture of ST-1040A and ST-1040B polyurethane [15] to make the UAV wing air tight. The open end of the UAV wing is attached to its cover with adhesives. The UAV wing is rolled along the span of the wing to condense it into a compact form as shown in Figure 19. The bounding dimensions of the folded UAV wing are 120 mm (length) x 70 mm (width) x 60 mm (height), whereas the bounding dimensions of the deployed UAV wing are 380 mm (length) x 100 mm (width) x 20 mm (height). The UAV wing is inflated successfully using an air pump at 1500 N/m² (gauge pressure), and the profile after inflation is shown in Figure 20.

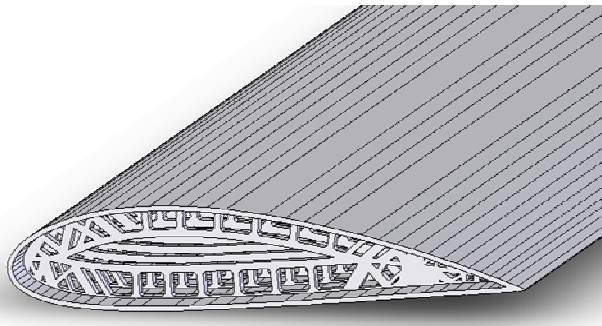


Figure 16. Cross-section of 3D CAD model of UAV wing.

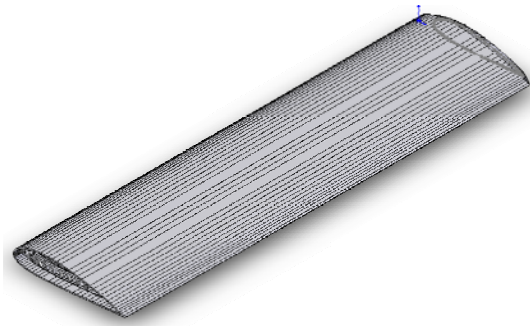


Figure 17. Isometric view of UAV CAD model.

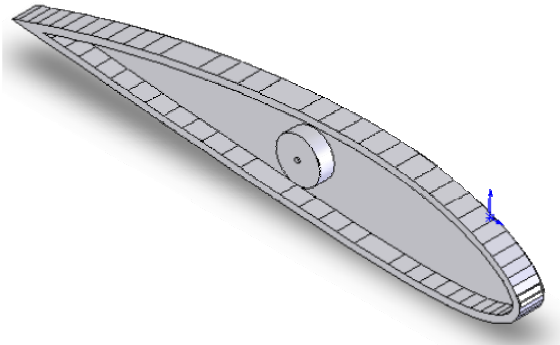


Figure 18. Cover to seal the open end of the UAV wing.

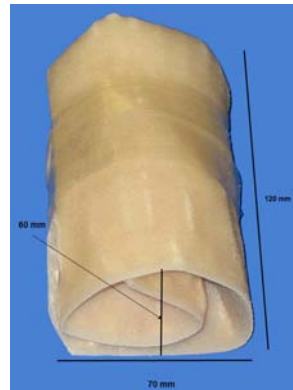


Figure 19. UAV wing in folded configuration.



Figure 20. UAV wing inflated using air pump at 1500N/m^2 (gauge pressure).

3. Closure

A methodology has been presented for deploying flexible, freeform structures with lattice skins as the deployment mechanism. In this paper, the focus has been primarily on the methodology for generating lattice structures and optimizing them so that the deployable structure maintains its profile after deployment. A ground structure approach for topology optimization of the lattice structure has been presented and applied to a representative, deployable UAV wing. By adjusting the lattice structure density and configuration, the topology optimization procedure resulted in a 78% improvement in maximum surface deflection when compared with a non-optimized structure. A physical prototype of the structure was fabricated with SLS and Duraform® FLEX material. It was successfully folded into a package with a maximum dimension of 120 mm, relative to a maximum dimension of 380 mm for the deployed wing. When coupled with prior feasibility studies, these results provide additional proof of concept for the use of lattice skins as deployment mechanisms.

Opportunities for ongoing work include increasing the comprehensiveness of the topology optimization procedure and formalizing post-processing steps for infiltrating and rigidizing deployed parts. For the UAV airfoil, the topology optimization procedure is performed in two dimensions for cross-sections of the lattice skin and then periodically repeated in the span direction. The lattice skin needs to be designed in three dimensions with characteristics such as fold-ability taken into account. For large structures, it may be necessary to reduce computational complexity by continuing to design the lattice skin in spatial segments, but more systematic methods for decomposing the problem are needed. With respect to post-processing, repeated infiltration with polyurethane appears to provide adequate short-term air tightness for pneumatic inflation, but further work is needed to identify thermoset polymers or other spray-on materials for rigidization and long-term stability of the deployed structure. Finally, it would be interesting to explore the possibility of virtually collapsing parts and fabricating them in their collapsed form, as a replacement for the current process of decomposing large parts into manufacturable pieces.

4. Acknowledgements

The authors gratefully acknowledge financial support from the University of Texas at Austin. The authors owe a special thanks to Jennifer Torkelson for her help with the Duraform® FLEX material and infiltrant and to the undergraduate students who participated in this project: Brian Nowotny, Trevor Page, Catherine Tradd and Brandon Walther.

5. References

1. Gantes, C. J., 2001, *Deployable Structures: Analysis and Design*, WIT Press, Boston.
2. Pellegrino, S., Ed., 2001, *Deployable Structures*, International Center for Mechanical Sciences, CISM Courses and Lectures No. 412, Springer-Verlag, New York.
3. Gibson, L. J. and M. F. Ashby, 1997, *Cellular Solids: Structure and Properties*, Cambridge University Press, Cambridge, UK.
4. Maheshwaraa, U., C. C. Seepersad and D. L. Bourell, 2007, "Design and Freeform Fabrication of Deployable Structures with Lattice Skins," *Rapid Prototyping Journal*, Vol. 13, No. 4, pp. 213-225.
5. Maheshwaraa, U., 2007, "Feasibility Study of Lattice Structure based Deployment Mechanism for Freeform Structures," *M.S. Thesis*, Mechanical Engineering, The University of Texas at Austin, Austin, TX.
6. ANSYS, 2006, ANSYS, Inc., Canonsburg, PA, Version 10.0.
7. iSIGHT, 2005, Engineous Software, Inc., Cary, NC, Version 9.0.
8. Kirsch, U., 1989, "Optimal Topologies of Structures," *Applied Mechanics Reviews*, Vol. 42, No. 8, pp. 223-239.
9. Topping, B. H. V., 1984, "Shape Optimization of Skeletal Structures: A Review," *Journal of Structural Engineering*, Vol. 109, No. 8, pp. 1933-1951.
10. Ohsaki, M. and C. C. Swan, 2002, "Topology and Geometry Optimization of Trusses and Frames," *Recent Advances in Optimal Structural Design* (S. A. Burns, Ed.), American Society of Civil Engineers, Reston, VA.
11. Dorn, W. S., R. E. Gomory and H. J. Greenberg, 1964, "Automatic Design of Optimal Structures," *Journal de Mecanique*, Vol. 3, pp. 25-52.
12. Abbott, I. H. and A. E. Von Doenhoff, 1959, *Theory of Wing Sections*, Dover Publications, Inc., New York.
13. Moran, J., 1984, *An Introduction to Theoretical and Computational Aerodynamics*, John Wiley and Sons, Inc., New York.
14. MATLAB, 2006, The Math Works, Inc., Natick, MA, Version 7.
15. <http://www.bjbenterprises.com/pdf/ST-3040.pdf>.